Chin. Phys. Lett. **39**, 030301 (2022)

Dynamics of the Entanglement Zero Modes in the Haldane Model under a Quantum Quench

Heng-Xi Ji(季亨茜)[1], Lin-Han Mo(莫林翰)[1], and Xin Wan(万歆)[1,2*]

[1]*Zhejiang Institute of Modern Physics, Zhejiang University, Hangzhou 310027, China*
[2]*CAS Center for Excellence in Topological Quantum Computation, University of Chinese Academy of Sciences, Beijing 100190, China*

(Received 4 December 2021; accepted 24 January 2022; published online 1 March 2022)

We investigate evolution of entanglement spectra of the Haldane model for Chern insulators upon a sudden quench within the same topological phase. In particular, we focus on the location of the entanglement spectrum crossing, which signifies the bulk topology. It is shown that the coplanarity condition for the pseudomagnetic field of the model, which can be used to determine the crossing in the equilibrium case, needs to be relaxed. We analytically derive the non-equilibrium condition with the help of an edge-state wave function ansatz and a dynamically induced length-scale cutoff. With spectral analyses, it is realized that the oscillatory behavior of the crossing is dominated by the interband excitations at the van Hove singularities.

DOI: 10.1088/0256-307X/39/3/030301

With recent experimental development, there is a growing interest in non-equilibrium dynamics of isolated quantum systems.[1−10] The simplest protocol is quantum quench,[11−15] which brings a sudden change to the Hamiltonian. In particular, Calabrese and Cardy introduced semiclassical quasiparticle excitations to describe the linear growth of entanglement entropy (EE) after a sudden quench.[16,17] This seems to suggest that details of quantum models, e.g., their band structures, are not important in a short time after the quench, apart from determining the prefactor of the linear growth.

On the other hand, one can find more information encoded in the so-called entanglement spectrum (ES), whose importance in identifying nonlocal properties, such as topology, of a static model was first emphasized by Li and Haldane.[18] Such an identification is possible due to the bulk-edge correspondence, which states, e.g. in the integer quantum Hall effect, that the bulk topological invariant[19] is tied to the number of edge states in a bounded system.[20] The edge states indeed manifest in the ES,[18,21,22] which can be computed through the eigenvalues of a reduced density matrix.

The marriage of topology and dynamics can bear apparently surprising results. For example, a quench from the topological to nontopological phase in the Haldane model[23] can have invariant Chern number in the thermodynamic limit, even though edge modes spread into the bulk and disappear in finite geometries.[24] In addition, symmetries respected by the initial wave function and the Hamiltonian at any time can be dynamically broken.[25] Consequently, the topological classification of noninteracting fermionic systems out of equilibrium differs from that in equilibrium, leading to important consequences in applications of zero modes in topological quantum computing.[26]

In the problem of identifying and detecting the topology of quench dynamics, Gong and Ueda[27] proposed that the time evolution of ES can be a universal indicator. In particular, the topological entanglement-spectrum crossings faithfully represent the topological classification in one dimension (1D) and are stable against disorder that preserves the corresponding symmetries. However, the generalization to higher dimensions is not obvious, as the extra dimensions introduce additional degrees of freedom that deserve scrutiny.

In two dimensions (2D), such a degree of freedom can be the characteristic momentum $k_{\rm c}$, at which 1D edge modes cross in the energy-momentum spectrum. In the Haldane model, Huang and Arovas[28] introduced an edge-state ansatz to compute $k_{\rm c}$ in the real-space edge spectrum. It turns out that, at $k_{\rm edge} = k_{\rm c}$, the pseudomagnetic field $\boldsymbol{B}$ in the Fourier-transformed Hamiltonian $H(\boldsymbol{k}) = W(\boldsymbol{k}) + \boldsymbol{B}(\boldsymbol{k})\cdot\boldsymbol{\sigma}$ lies on a plane that contains the origin, and therefore, the bulk Chern index is reduced to the winding number of $\boldsymbol{B}$. Not surprisingly, both the entanglement spectrum and the Wannier centers exhibit crossings at the same $k_{\rm c}$.[28]

In this Letter, we investigate evolution of topological entanglement spectra crossing in the quench dynamics of the 2D Haldane model. After a sudden

*Corresponding author. Email: xinwan@zju.edu.cn
© 2022 Chinese Physical Society and IOP Publishing Ltd

quench in the same topological phase, the pseudomagnetic field precesses about $\boldsymbol{k}$-dependent axis at each momentum. The topological structure is no longer associated with the coplanarity of $\boldsymbol{B}$ at $k_{\rm c}$, but with a relaxed condition. Consequently, $k_{\rm c}$ develops an oscillation that has multiple spectral peaks, which correspond to interband transitions at the van Hove singularities.

Haldane's 2D honeycomb model describes spinless fermions hopping on a lattice with a staggered magnetic field. The Hamiltonian is given by[23]

$$\begin{aligned}\hat{H} =& -t_0\sum_{\langle i,j\rangle}\left(\hat{c}_i^\dagger\hat{c}_j+\text{H.c.}\right)\\ &-t_1\sum_{\langle\langle i,j\rangle\rangle}\left(e^{i\phi_{ij}}\hat{c}_i^\dagger\hat{c}_j+\text{H.c.}\right)\\ &+M\Big(\sum_{i\in A}\hat{n}_i-\sum_{i\in B}\hat{n}_i\Big),\end{aligned}\tag{1}$$

where $\hat{c}_i$, $\hat{c}_j^\dagger$ are fermionic operators, $\hat{n}_i\equiv\hat{c}_i^\dagger\hat{c}_i$; t_0 and $t_1e^{i\phi_{ij}}=t_1e^{\pm i\phi}$ are nearest and next-nearest neighbor hopping strengths; the latter breaks the time-reversal symmetry. The energy offsets M and $-M$ on A and B sublattices, respectively, break the sublattice symmetry. We choose primitive vectors $\boldsymbol{a}_1$ and $\boldsymbol{a}_2$ with corresponding momenta k_1 and k_2 as illustrated in Fig. 1(a) and set $t_0=1$ and $t_1=1/3$ for concreteness.

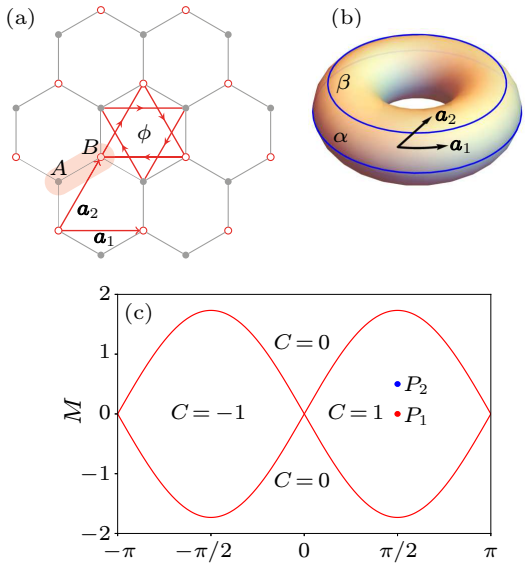

Fig. 1. (a) Two-dimensional honeycomb lattice and our choice of the primitive vectors for the Haldane model. (b) The system with periodic boundary conditions on a torus geometry. To calculate the OPES, we partition the system along $\boldsymbol{a}_1$ (blue lines) into subsystems α and β with zigzag edges. (c) The phase diagram of the model with topological phases ($C=\pm1$) surrounded by non-topological phases ($C=0$). We focus on the quantum quench from $P_1(M=0,\phi=\pi/2)$ to $P_2(M=0.5,\phi=\pi/2)$ as marked by the red and blue points, respectively.

The bulk Hamiltonian in momentum space is $H(k_1,k_2)=W(k_1,k_2)+\boldsymbol{B}(k_1,k_2)\cdot\boldsymbol{\sigma}$, where $\boldsymbol{B}=(B_x,B_y,B_z)$ is a pseudomagnetic field, and $\boldsymbol{\sigma}=(\sigma_x,\sigma_y,\sigma_z)$ are Pauli matrices for subband isospin. Explicitly,

$$\begin{aligned}B_x &= -1-\cos k_1-\cos k_2,\\ B_y &= \sin k_1+\sin k_2,\\ B_z &= M+\frac{2}{3}\sin\phi\,[\sin k_1-\sin k_2+\sin(k_2-k_1)],\\ W &= -\frac{2}{3}\cos\phi\,[\cos k_1+\cos k_2+\cos(k_2-k_1)].\end{aligned}\tag{2}$$

The energy of the two-band model is $E_\pm(k_1,k_2)=W(k_1,k_2)\pm|\boldsymbol{B}(k_1,k_2)|$. We consider the model at half filling, such that $|\Psi_{\rm gs}\rangle=\Pi_{l.b.}\hat{c}^\dagger_{k_1,k_2}|0\rangle$. The ground state can be characterized by a Chern number $C=\frac{1}{2}[\text{sgn}(m)-\text{sgn}(m')]$ with effective masses $m=M+\sqrt{3}\sin\phi$ and $m'=M-\sqrt{3}\sin\phi$. The phase diagram of the Haldane model at half filling is shown in Fig. 1(c), which consists of two topological phases ($C=\pm1$) and a trivial phase ($C=0$).

The system is partitioned along $\boldsymbol{a}_1$ direction into subsystems α and β, as shown in Fig. 1(b). In such a free-fermion system, the entanglement spectrum can be obtained from the correlation matrix restricted in the subsystem α (i.e., $n,m\in\alpha$) as $C_{mn}=\langle\Psi_{\rm gs}|\hat{c}_m\hat{c}_n^\dagger|\Psi_{\rm gs}\rangle$.[29,30] At half filling, one can show that the correlation matrix in k space is

$$C(k_1,k_2)=\frac{\mathbb{I}}{2}+\frac{\hat{\boldsymbol{B}}(k_1,k_2)\cdot\boldsymbol{\sigma}}{2},\tag{3}$$

where $\hat{\boldsymbol{B}}=\boldsymbol{B}/|\boldsymbol{B}|$ can be obtained from Eq. (2). The eigenvalues λ_n of the restricted correlation matrix is known as the one-particle entanglement spectrum (OPES), which is related to the quadratic entanglement Hamiltonian $H_{\rm E}=\sum_n\epsilon_n\hat{f}_n^+\hat{f}_n$ through $\lambda_n=1/(e^{\epsilon_n}+1)$. Examples of the OPES are shown in Fig. 2(a) for two sets of (M,ϕ), labeled as P_1 and P_2 in Fig. 1(c). Here, we illustrate with a system having $L_2=400$ unit cells along $\boldsymbol{a}_2$ and a subsystem α with $L_2'=L_2/2$. The hallmark of the OPES for the topologically nontrivial states is the counter-propagating edge modes that cross at a characteristic $k_{\rm c}$, at which $\lambda_n=1/2$. The two degenerate modes are entanglement zero modes, as their corresponding entanglement energy $\epsilon_n=0$.

As emphasized in Ref. [28], in the equilibrium case, the entanglement spectrum crossing or the half-occupancy mode ($\lambda=1/2$) occurs at the same $k_{\rm c}$ of the edge spectrum crossing point and the half-odd-integer Wannier center. For the Haldane model, one has explicitly $\sin k_{\rm c}=-M/(2\sin\phi)$. One can verify that the entanglement spectrum crossing occurs at $k_1=k_{\rm c}$, at which the coplanarity condition of the pseudomagnetic field $\boldsymbol{B}$ is satisfied, i.e.,

$$[\hat{\boldsymbol{B}}(k_{\rm c},k_2)\times\hat{\boldsymbol{B}}(k_{\rm c},k_2')]\cdot\hat{\boldsymbol{B}}(k_{\rm c},k_2'')=0,\tag{4}$$

for arbitrary k_2, k_2', k_2''. Examples of $\hat{\boldsymbol{B}}$ at and away from k_c are illustrated on a Bloch sphere in Fig. 2(b). As expressed by Eq. (4), the line swept by the end of $\hat{B}(k_c, k_2)$ encircles the origin, as shown in Fig. 2(b), thus can be mapped to a topologically nontrivial one-dimensional model.[28]

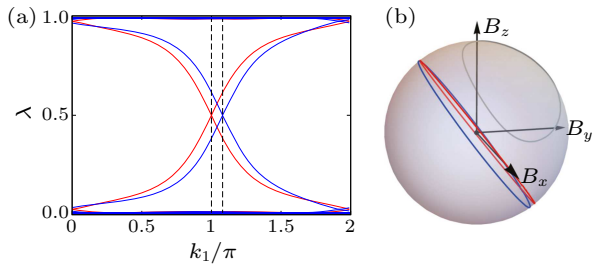

Fig. 2. (a) Equilibrium OPES of the half-filled system with $L_2 = 400$ at P_1 (red curves) and P_2 (blue curves) in Fig. 1(c). The edge modes of the $L_2' = 200$ subsystem α cross at $k_c = \pi$ and $\pi + \sin^{-1} 0.25 \approx 1.08\pi$, respectively. (b) At the crossing points, the normalized pseudomagnetic field $\hat{B}(k_c, k_2)$ is coplanar and sweeps a great circle (red and blue curves) that encloses the origin at its center. The gray curve illustrates a trace of $\hat{B}$ away from k_c.

We now consider the dynamical case under a quantum quench, e.g., a sudden change of the Hamiltonian from H to H' (represented by P_1 and P_2, respectively) at $t = 0$. The state of the system evolves unitarity as $|\Psi_{\rm gs}(t)\rangle = e^{-iH't}|\Psi_{\rm gs}\rangle$, where we set $\hbar = 1$. The time-dependent correlation matrix in the k space has a 2×2 form as

$$C(t, k_1, k_2) \equiv \begin{pmatrix} C^{\rm AA} & C^{\rm AB} \\ C^{\rm BA} & C^{\rm BB} \end{pmatrix} = \frac{\mathbb{I}}{2} + \frac{\hat{\boldsymbol{B}}(t, k_1, k_2)\cdot\boldsymbol{\sigma}}{2}, \tag{5}$$

where $\hat{\boldsymbol{B}}(t)$ is the dynamical pseudomagnetic field, which can be regarded as the pre-quench $\hat{\boldsymbol{B}}$ precessing about the post-quench $\hat{\boldsymbol{B}}'$ with a Larmor frequency $2|\boldsymbol{B}'|$. Explicitly, we can express $\hat{\boldsymbol{B}}(t)$ as the sum of three mutually orthogonal vectors:

$$\begin{aligned}\hat{\boldsymbol{B}}(t) = {}& \cos(2|\boldsymbol{B}'|t)(\hat{\boldsymbol{B}} - (\hat{\boldsymbol{B}}\cdot\hat{\boldsymbol{B}}')\hat{\boldsymbol{B}}') \\ & + \sin(2|\boldsymbol{B}'|t)(\hat{\boldsymbol{B}}\times\hat{\boldsymbol{B}}') + (\hat{\boldsymbol{B}}\cdot\hat{\boldsymbol{B}}')\hat{\boldsymbol{B}}'. \end{aligned}\tag{6}$$

Therefore, the calculation of the dynamical OPES is technically identical to that in the equilibrium case.

In each k_1 block, the correlation matrix has a form

$$\tilde{C}(t, k_1) \equiv \begin{pmatrix} \tilde{C}^{\rm AA} & \tilde{C}^{\rm AB} \\ \tilde{C}^{\rm BA} & \tilde{C}^{\rm BB} \end{pmatrix}, \tag{7}$$

where the matrix element is the Fourier transform of the corresponding element of $C(t, k_1, k_2)$,

$$\tilde{C}^{\rm AA}_{nm} = \frac{1}{2\pi}\int dk_2 e^{ik_2(n-m)} C^{\rm AA}, \tag{8}$$

and similarly for $\tilde{C}^{\rm AB} = (\tilde{C}^{\rm BA})^\dagger$ and $\tilde{C}^{\rm BB}$. The superscripts are defined similarly as in Eq. (5). We calculate the time-dependent OPES for the system with $L_2 = 400$, as shown in Fig. 3(a) at $t = 10$. Even though the edge modes show clear wiggles, the spectrum exhibits a well-defined crossing at $k_c(t) \approx 1.07\pi$. As demonstrated in Fig. 3(b), the coplanarity condition for $\hat{B}(t)$ is clearly violated in the dynamical case.

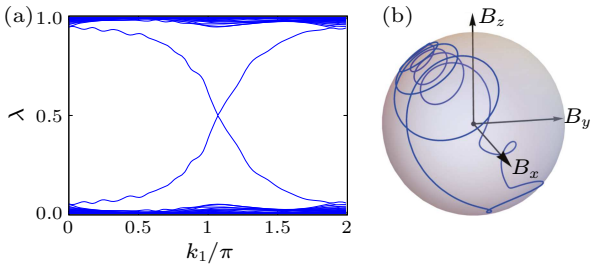

Fig. 3. (a) Non-equilibrium OPES at $t = 10$, after the system with $L_2 = 400$ quenches from P_1 to P_2 in the phase diagram [Fig. 1(c)] at $t = 0$. The spectrum still features a well-defined crossing at $k_c(t) \approx 1.07\pi$, but the edge modes show clear wiggles. (b) Even at the crossing point, the dynamical pseudomagnetic field $\hat{\boldsymbol{B}}(t)$ is no longer coplanar but winds around the Bloch sphere.

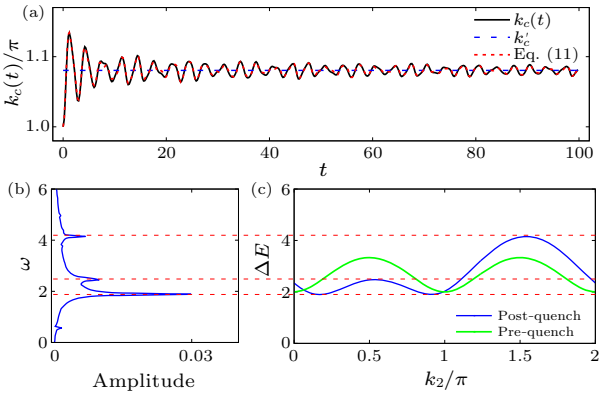

Fig. 4. (a) Evolution of $k_c(t)$ in the system with $L_2 = 400$ after the quench from P_1 to P_2 for $t < 100$. Here $k_c(t)$ oscillates around the post-quench equilibrium k_c' (blue dashed line). The red curve is obtained from Eq. (11). (b) The corresponding frequency spectrum of $k_c(t)$. (c) The interband excitation energy ΔE at the corresponding crossing points for the pre- (green curve) and post-quench (blue curve) Hamiltonians. The dashed lines mark the post-quench $\Delta E = 2|\boldsymbol{B}'|$ of the van Hove singularities in (c), which coincide with the spectral peaks in (b).

Figure 4(a) plots the evolution of $k_c(t)$ after the quench for $0 < t < 100$. Note that in the Calabrese–Cardy picture[16,17] quasiparticles travel with velocity $v_2 = {\rm d}E/{\rm d}k_2$ after the quench, which defines a characteristic time $t_c = L_2/(2v_{2,\max}) \simeq 111$ in our system, so we stay away from the interference of quasiparticles or the revival of the pre-quench state.[31] The entanglement spectrum crossing starts from the pre-quench $k_c = \pi$ and oscillates around the post-quench $k_c' = 1.08\pi$ with a decreasing amplitude. The Fourier transformation of $k_c(t)$ is shown in Fig. 4(b), which exhibits three sharp peaks in the frequency space. For comparison, we plot the interband excitation energy $\Delta E = 2|\boldsymbol{B}|$ at the entanglement spectrum crossing

points for both the pre- and post-quench systems in Fig. 4(c). One can see that the peaks in Fig. 4(b) match the excitation energies at the van Hove singularities of the post-quench dispersion. Therefore, we find numerically that the oscillatory location of $k_c(t)$ is dominated by the interband excitations at the van Hove singularities.

To analytically calculate k_c in the non-equilibrium case, we follow the Huang–Arovas ansatz[28] to postulate that the edge states of the time-dependent correlation matrix have solutions in the form of $(\psi_A, \psi_B) = (\psi, \gamma\psi)$; in other words, the wave function on the A sublattice ψ_A has the same (presumably decaying) form ψ as that on the B sublattice ψ_B, up to a numerical factor γ. This can appear when

$$\tilde{C}^{AA} + \gamma\tilde{C}^{AB} - \lambda\mathbb{I} = r(\tilde{C}^{BB} + \gamma^{-1}\tilde{C}^{BA} - \lambda\mathbb{I}), \quad (9)$$

where r is another numerical factor to be determined. For a given k_1 and sufficiently large t, $\hat{B}(t)$ winds around the Bloch sphere rapidly as k_2 changes, as illustrated in Fig. 3(b). In fact, the number of turns increases with t. As a consequence, the matrix elements of the correlation matrix in Eq. (8) are dominated by $n - m = 0$ and ± 1, so we can approximate each block of $\tilde{C}$ by a tridiagonal matrix. Hence, Eq. (9) is reduced to

$$\begin{aligned} &\frac{\tilde{C}^{AA}_{00} + \gamma\tilde{C}^{AB}_{00} - \lambda}{\tilde{C}^{BB}_{00} + \gamma^{-1}\tilde{C}^{AB}_{00} - \lambda} = \frac{\tilde{C}^{AA}_{10} + \gamma\tilde{C}^{AB}_{10}}{\tilde{C}^{BB}_{10} + \gamma^{-1}\tilde{C}^{AB}_{10}} \\ &= \frac{\tilde{C}^{AA}_{01} + \gamma\tilde{C}^{AB}_{01}}{\tilde{C}^{BB}_{01} + \gamma^{-1}\tilde{C}^{AB}_{01}} = r. \end{aligned} \quad (10)$$

Notably we have two degenerate $\lambda = 1/2$ the entanglement spectrum crossing point, at which γ and r in Eq. (10) are overdetermined. The condition that we can find a solution, as clearly supported by the numerical calculation, can be obtained with a procedure described in Ref. [28] for the crossing point in the edge spectrum. After lengthy but straightforward algebras, we arrive at the following triple-integral condition

$$\begin{aligned} &\int \mathrm{d}k_2\mathrm{d}k_2'\mathrm{d}k_2''[\sin(k_2 - k_2') + \sin(k_2' - k_2'') \\ &+ \sin(k_2'' - k_2)] \times \{[\hat{\boldsymbol{B}}(t, k_c(t), k_2) \times \hat{\boldsymbol{B}}(t, k_c(t), k_2')] \\ &\cdot \hat{\boldsymbol{B}}(t, k_c(t), k_2'')\} = 0, \end{aligned} \quad (11)$$

where $\hat{\boldsymbol{B}}(t, k_1, k_2)$ is defined in Eq. (6) for the dynamical case. The result can be regarded as the relaxation of the equilibrium coplanarity condition at k_c to the non-equilibrium case. The stronger coplanarity condition in Eq. (4) reincarnates now as a time-dependent factor in the integrand, which is modulated by a static geometrical factor that depends only on momenta, but not the band structure.

Based on Eq. (11), we determine $k_c(t)$ and plot it in Fig. 4(a). The result overlaps perfectly with that obtained from the direct numerical calculation of the OPES, which implies that the edge-state ansatz wave function and the tridiagonal approximation of the correlation matrix are well justified. Equation (11) also provides an explanation why the spectral analysis of $k_c(t)$ is dominated by the excitation energies at the van Hove singularities. The dynamical $\hat{\boldsymbol{B}}(t)$, as defined in Eq. (6), has fast oscillating terms $\cos(2|\boldsymbol{B}'|t)$ and $\sin(2|\boldsymbol{B}'|t)$, whose frequency corresponds to the interband excitation energy $\Delta E = 2|\boldsymbol{B}'|$ for the post-quench system. Hence, the oscillatory integrand in Eq. (11) contributes significantly only at the van Hove singularities, in the vicinity of which the contributions interfere constructively in the determination of $\Delta k_c(t) = k_c(t) - k_c'$. Meanwhile, the non-oscillating term in Eq. (6) dictates the long-time behavior $k_c(t) = k_c'$.

We also study the dynamics of the entanglement zero modes under quenches between other pairs of parameters. It is found that the decaying oscillations of $k_c(t)$ manifest in general, which can also be compared to the interband excitation energy at the van Hove singularities. It is possible that additional pairs of zero-mode crossings can emerge in the dynamical entanglement spectrum. This, however, is not a violation of the correspondence to the bulk topology, as the crossings appear in pairs so their number parity is preserved. Such a scenario of emergent crossings also occurs when we quench the system from the $C = 1$ to $C = -1$ topological phase.[31] The dynamics of these additional modes will be analyzed in our future study, which falls under the subject of bulk and edge phase transitions.

In summary, we focus on the entanglement spectrum crossing $k_c(t)$ of the Haldane model under a quantum quench within the same topologically nontrivial phase. Due to the precession of the pseudomagnetic field, high-frequency components in the correlation matrix are suppressed. The coplanarity condition for the entanglement spectrum crossing in the equilibrium case is now relaxed to a triple-integral condition for $k_c(t)$. Consequently, $k_c(t)$ oscillates around its post-quench equilibrium value with decreasing amplitude. The frequency spectrum of $k_c(t)$ is dominated by the interband transitions at the van Hove singularities, whose contributions to the triple integral are stationary.

The existence of the entanglement edge-state crossing, or the pair of zero modes, is a manifestation of the bulk topology. In the quantum quench within the same topologically nontrivial phase, the dynamical system remains to be nontrivial and preserves the midgap entanglement spectral crossing. However, the location of the dynamical zero modes is not topological and can oscillate before it relaxes to the post-quench equilibrium value. We can, therefore, attribute the lo-

cation information to be geometrical. This also manifests in the analytical solution in Eq. (11), in which the triple product of the dynamical pseudomagnetic magnetic field is integrated with a particular geometrical factor, which arises from the dominance of short length scales in the correlation matrix. Therefore, the study of the dynamics of the entanglement zero modes reveals the interesting and intricate interplay of topology and geometry in non-equilibrium quench dynamics.

Acknowledgments. The authors thank Lih-King Lim for helpful discussion and the critical reading of a previous version. This work was supported in part by the National Natural Science Foundation of China (Grant No. 11674282), and the Strategic Priority Research Program of Chinese Academy of Sciences (Grant No. XDB28000000).

References

[1] Kinoshita T, Wenger T and Weiss D S 2006 *Nature* **440** 900
[2] Hofferberth S, Lesanovsky I, Fischer B, Schumm T and Schmiedmayer J 2007 *Nature* **449** 324
[3] Trotzky S, Chen Y A, Flesch A, McCulloch I P, Schollwöck U, Eisert J and Bloch I 2012 *Nat. Phys.* **8** 325
[4] Gring M, Kuhnert M, Langen T, Kitagawa T, Rauer B, Schreitl M, Mazets I, Smith D A, Demler E and Schmiedmayer J 2012 *Science* **337** 1318
[5] Cheneau M, Barmettler P, Poletti D, Endres M, Schauss P, Fukuhara T, Gross C, Bloch I, Kollath C and Kuhr S 2012 *Nature* **481** 484
[6] Meinert F, Mark M J, Kirilov E, Lauber K, Weinmann P, Daley A J and Nägerl H C 2013 *Phys. Rev. Lett.* **111** 053003
[7] Langen T, Geiger R, Kuhnert M, Rauer B and Schmiedmayer J 2013 *Nat. Phys.* **9** 640
[8] Fukuhara T, Kantian A, Endres M, Cheneau M, Schauß P, Hild S, Bellem D, Schollwöck U, Giamarchi T, Gross C, Bloch I and Kuhr S 2013 *Nat. Phys.* **9** 235
[9] Fukuhara T, Schauß P, Endres M, Hild S, Cheneau M, Bloch I and Gross C 2013 *Nature* **502** 76
[10] Langen T, Erne S, Geiger R, Rauer B, Schweigler T, Kuhnert M, Rohringer W, Mazets I E, Gasenzer T and Schmiedmayer J 2015 *Science* **348** 207
[11] Polkovnikov A, Sengupta K, Silva A and Vengalattore M 2011 *Rev. Mod. Phys.* **83** 863
[12] Gogolin C and Eisert J 2016 *Rep. Prog. Phys.* **79** 056001
[13] Vidmar L and Rigol M 2016 *J. Stat. Mech.* **2016** 064007
[14] Essler F H L and Fagotti M 2016 *J. Stat. Mech.* **2016** 064002
[15] Calabrese P and Cardy J 2016 *J. Stat. Mech.* **2016** 064003
[16] Calabrese P and Cardy J 2005 *J. Stat. Mech.* **2005** P04010
[17] Calabrese P and Cardy J 2006 *Phys. Rev. Lett.* **96** 136801
[18] Li H and Haldane F D M 2008 *Phys. Rev. Lett.* **101** 010504
[19] Thouless D J, Kohmoto M, Nightingale M P and den Nijs M 1982 *Phys. Rev. Lett.* **49** 405
[20] Hatsugai Y 1993 *Phys. Rev. Lett.* **71** 3697
[21] Swingle B and Senthil T 2012 *Phys. Rev. B* **86** 045117
[22] Qi X L, Katsura H and Ludwig A W W 2012 *Phys. Rev. Lett.* **108** 196402
[23] Haldane F D M 1988 *Phys. Rev. Lett.* **61** 2015
[24] Caio M D, Cooper N R and Bhaseen M J 2015 *Phys. Rev. Lett.* **115** 236403
[25] McGinley M and Cooper N R 2018 *Phys. Rev. Lett.* **121** 090401
[26] McGinley M and Cooper N R 2019 *Phys. Rev. B* **99** 075148
[27] Gong Z and Ueda M 2018 *Phys. Rev. Lett.* **121** 250601
[28] Huang Z and Arovas D P 2012 arXiv:1205.6266 [cond-mat.str-el]
[29] Chung M C and Peschel I 2001 *Phys. Rev. B* **64** 064412
[30] Peschel I 2003 *J. Phys. A* **36** L205
[31] Mo L H, Zhang Q L and Wan X 2020 *Chin. Phys. Lett.* **37** 060301